Applied Physics Letters

Exploring leakage in dielectric films via automated experiments in scanning probe microscopy

Cite as: Appl. Phys. Lett. **120**, 182903 (2022); https://doi.org/10.1063/5.0079217
Submitted: 18 November 2021 • Accepted: 19 April 2022 • Published Online: 05 May 2022

Yongtao Liu, Shelby S. Fields, Takanori Mimura, et al.

Exploring leakage in dielectric films via automated experiments in scanning probe microscopy

Cite as: Appl. Phys. Lett. **120**, 182903 (2022); doi: 10.1063/5.0079217
Submitted: 18 November 2021 · Accepted: 19 April 2022 ·
Published Online: 5 May 2022

View Online Export Citation CrossMark

Yongtao Liu,[1] Shelby S. Fields,[2] Takanori Mimura,[2] Kyle P. Kelley,[1] Susan Trolier-McKinstry,[3,4] Jon F. Ihlefeld,[2,5] and Sergei V. Kalinin[6,a)]

AFFILIATIONS

[1]Center for Nanophase Materials Sciences, Oak Ridge National Laboratory, Oak Ridge, Tennessee 37831, USA
[2]Department of Materials Science and Engineering, University of Virginia, Charlottesville, Virginia 22904, USA
[3]Center for Dielectrics and Piezoelectrics, Materials Research Institute, The Pennsylvania State University, University Park, Pennsylvania 16802, USA
[4]Department of Materials Science and Engineering, The Pennsylvania State University, University Park, Pennsylvania 16802, USA
[5]Charles L. Brown Department of Electrical and Computer Engineering, University of Virginia, Charlottesville, Virginia 22904, USA
[6]Department of Materials Science and Engineering, University of Tennessee, Knoxville, Tennessee 37923, USA

[a)]Author to whom correspondence should be addressed: sergei2@utk.edu

ABSTRACT

Electronic conduction pathways in dielectric thin films are explored using automated experiments in scanning probe microscopy (SPM). Here, we use large field of view scanning to identify the position of localized conductive spots and develop an SPM workflow to probe their dynamic behavior at higher spatial resolution as a function of time, voltage, and scanning process in an automated fashion. Using this approach, we observe the variable behaviors of the conductive spots in a 20-nm-thick ferroelectric $Hf_{0.54}Zr_{0.48}O_2$ film, where conductive spots disappear and reappear during continuous scanning. There are also fresh conductive spots that develop during scanning. The automated workflow is universal and can be integrated into a wide range of microscopy techniques, including SPM, electron microscopy, optical microscopy, and chemical imaging.

Oxide films are utilized in various applications in the semiconductor industry. Passive dielectric films are broadly used as gate dielectrics or as sacrificial layers during semiconductor processing. Functional oxides such as ferroelectrics and antiferroelectrics are used for tunable microwave elements, and information or energy storage.[1–3] Therefore, interest in ferroelectric thin films grew from the 1980s to the early 2000s. However, traditional perovskite-based ferroelectrics are difficult to integrate into semiconductor processing technology due to the thermodynamic instability of the ferroelectric–semiconductor interface, coupled with high process temperatures and limited thickness scaling.[4] Recently, the discovery of ferroelectricity in hafnium oxide-based materials has increased research in this area due to their compatibility with semiconductor nanofabrication processes and the presence of robust ferroelectricity in very thin films.[5–7]

However, thin dielectric and ferroelectric films are susceptible to the formation of conductive pathways.[8–11] These pathways can be detrimental to device performance, as leaks develop in the film, necessitating mitigation. Conversely, these pathways can potentially improve the function of resistive switching devices. Therefore, studying the formation and behavior of conductive pathways in thin-film ferroelectrics will be useful for the future development of this class of materials.

Scanning probe microscopy (SPM) is an ideal tool to study the local conductivity of thin film materials.[12–15] Lau *et al.* investigated conductance switching in metal/molecule/metal structures by measuring the local junction conductance via SPM.[16,17] They demonstrated that device switching arises from the appearance and disappearance of nanoscale conducting spots. Yang *et al.* investigated local conductive channels in other memristor devices and their effects on device performance.[18] Using conductive SPM,[19] Szot *et al.* demonstrated that the switching behavior of single-crystalline $SrTiO_3$ originates from the local modulation of defects. These local defects can act as bistable nanowires, a useful component in terabit memory devices. Conductive spots, channels, and defects are often spatially separated, meaning that they appear localized in large field of view (FoV) microscopy images. In order to study conductive spots in detail with current technology, the zoom-in process must be operated manually, involving human intervention to determine the scan-in parameters, e.g., zoom-in location, scan size, etc. An automated zoom-in process, driven by computers, is desirable.

Therefore, we developed an automated workflow for SPM (feature-exploration workflow) that enables the exploration of specific features in microscopy images. This expands upon previous work on controlled tip trajectories[20] and automated experiments in piezoresponse force microscopy (PFM).[21–26] In feature-exploration workflow, the features of interest in microscopy images are automatically discovered and located. Then, the zoom-in process is performed in an automatic manner according to the parameters of each feature, e.g., the feature size and shape. When studying conductive spots in thin films, the feature-exploration workflow is integrated with conductive atomic force microscopy (FE-cAFM, abbreviated as cAFM) to investigate local conductivity. It is notable that feature-exploration workflow is universal and compatible with other microscopies.

We integrated feature-exploration workflow with cAFM to investigate the local conductivity of a 20-nm-thick crystalline $Hf_{0.54}Zr_{0.48}O_2$ (HZO) thin film prepared atop a TaN electrode on silicon.[27,28] The preparation of the HZO film is illustrated in Methods in the supplementary material. The film's topography and cAFM current images are shown in Fig. 1. The large FoV topography image in Fig. 1(b) shows the overall morphology, while the small FoV topography image in Fig. 1(c) shows the film's grain structures. The cAFM current image in Fig. 1(d) displays several highly conducting spots (red spots); they are small (around several tens of nanometers) and randomly distributed.

To explore the structure and functionality of conductive hot-spots in an automated fashion, we developed a feature-exploration workflow enabling the entire measurement process (from the large FoV scan to small FoV zoom-in scans) to be driven by computer. Furthermore, the FoV can be customized by users to meet the specific needs of their research. The computer controls the zoom-in measurements according to the location and size of the features under investigation; it generates zoom-in parameters such as location (x_i, y_i), scan size (s_i), scan rate (r_i), etc. It then records and saves all results from the zoom-in measurements. The decision making for zoom-in parameters is worth further improvement in the future,[29] e.g., including functions to actively adjust these parameters according to the information acquired from the zoom-in measurement. Figure 2(a) shows a schematic of the feature-exploration workflow in our study. A large FoV cAFM measurement was taken first. Then, the conductive hot spot identification process was realized via object-segmentation from the background by a threshold filter. Figure 2(b) shows how we implemented this workflow in our SPM, where a field-programmable gate array (FPGA) was connected to the SPM software for real-time control and data acquisition. Here, we use an Oxford Instrument Asylum Cypher SPM and a National Instruments USB-7865R R Series Multifunction RIO FPGA for the automated measurement. The FPGA sends the piezo-voltage to the piezo-X and piezo-Y channels of the SPM controller to move the tip to desired locations and performs scanning.

We investigated the conductive spots in the HZO thin film via FE-cAFM; the results are shown in Fig. 3. Figure 3(a) shows four conductive spots in a large FoV cAFM current image. The locations of these conductive spots were determined by the feature-exploration workflow, where the marked boxes represent the zoom-in measurement regions. These are shown in Fig. 3(b). Figure 3(c) shows the zoom-in cAFM results, which illustrate the evolution of the conductive spots as a function of scan cycle in the continuous scan process. Interestingly, the four spots show different behaviors. The first and second conductive spots appear as two separate spots after zoom-in; their shape and size change throughout the continuous scan. The second conductive spot disappears in the fourth and fifth zoom-in image [Fig. 3(c-2)]. A similar phenomenon can also be observed in the zoom-in results of the first conductive spot [Fig. 3(c-1)], where the conductive spot is very weak in the fourth zoom-in image; however, it becomes stronger again in the fifth zoom-in image. The third conductive spot [Fig. 3(c-3)] is very weak in the zoom-in images, consistent

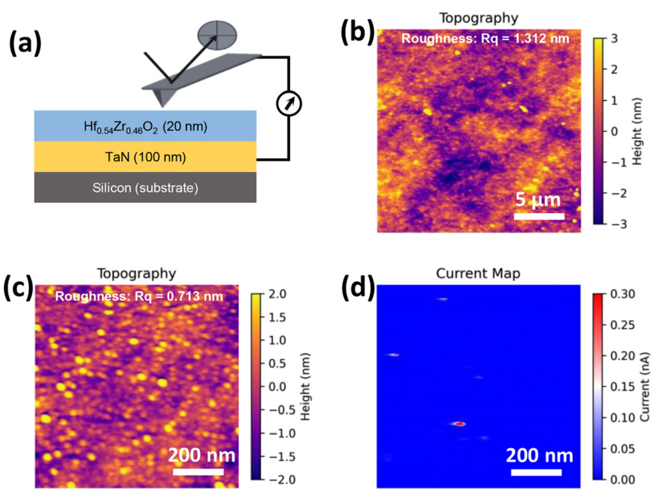

FIG. 1. cAFM results of the HZO thin film. Schematic of (a) device structure and conductive AFM measurement; (b) a large FoV topography image, and the roughness of this topography is 1.312 nm; (c) a small FoV topography image, and the roughness of this topography is 0.713 nm; and (d) a cAFM current image corresponding to the small FoV topography in (b).

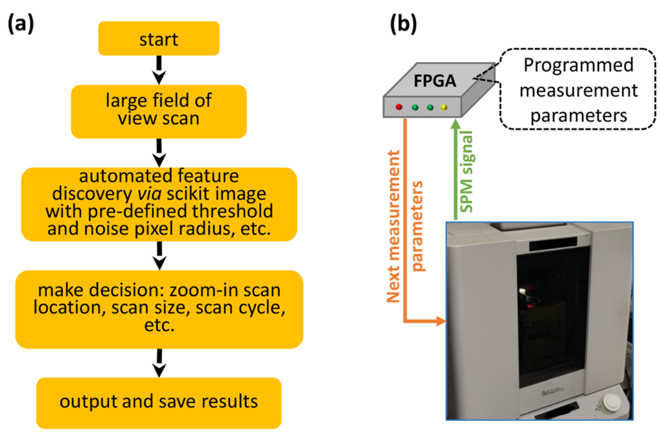

FIG. 2. Schematic of the automated feature-exploration workflow. (a) Detailed workflow. In the feature discovery process, a predefined thresholding value (according to the conductivity of the conductive spots) is used to turn the cAFM image to binary and subsequently find the contours of the features in the binary image; note that two approaches of finding the contours of the desired features are provided in the Python notebook. (b) A scheme showing the intervention between computer and microscope.

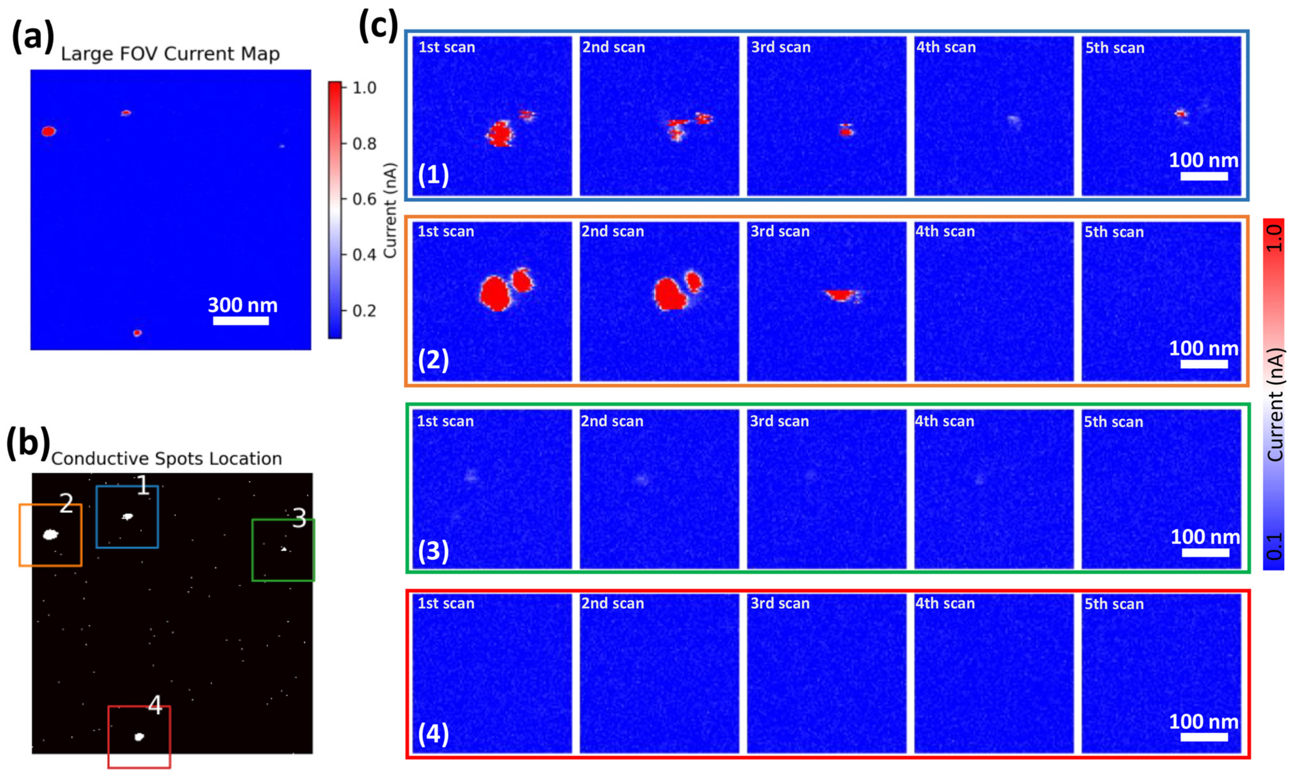

FIG. 3. FE-cAFM results of the HZO thin film by applying $V_{DC} = 6.7$ V. (a) Large FoV current map. (b) Conductive spot locations determined by FE workflow. (c) Zoomed-in scan results showing the behavior of each conductive spot as a function of scan cycle.

with its behavior in the large FoV image [Fig. 3(a)]. Interestingly, the fourth conductive spot completely disappears in the zoom-in images [Fig. 3(c-4)]. Given the measurement sequence of Fig. 3(c) is (1)→(2)→(3)→(4), the appearance of conductive spots is observed after the disappearance in some cases; therefore, the disappearance of the conductive spots is unlikely to be due to tip degradation. This FE-cAFM result reveals that the behaviors of the conductive spots in this HZO thin film are different in some cases; that is, some become progressively smaller and then larger, while others disappear in subsequent datasets.

We also studied the evolution of conductive spots as a function of applied DC voltage. The results are shown in Fig. 4. Figure 4(a) shows the cAFM current images under continuous scan with a constant $V_{dc} = 7.0$ V, where the conductive spots gradually appear and/or disappear during scanning. Figure 4(b) shows the *in situ* cAFM current map with an increase $V_{dc} = 7.2$ V; more conductive spots are visible compared to the current map in Fig. 4(a). In addition, most spots appear larger. The second scan in Fig. 4(b) shows an increase in the number and density of the conductive spots as compared to the first scan. When the V_{dc} was increased to 7.4 V [first scan in Fig. 4(c)], an increase in the number and size of the conductive spots occurred. However, in the second scan under 7.4 V in Fig. 4(c), a significant change in the shape of the spots occurred.

To investigate the change in shape of the spots, we performed FE-cAFM measurements on the cAFM image in the second scan under $V_{dc} = 7.4$ V [Fig. 4(c)]. The results are shown in Fig. 5. Figure 5(a) shows a copy of the second scan of Fig. 4(c), which was used as the large FoV current image for FE-cAFM—this suggests that the feature-exploration workflow can be used anytime during SPM measurement. Figure 5(b) shows the locations of the conductive spots. We changed the parameter of spot size in the feature-exploration workflow, so only relatively large spots were located in Fig. 5(b). Figure 5(c) shows the zoom-in current images, which reveal the shape of the conductive spots. Interestingly, the "spots" in Fig. 5(c) show a ring shape. Careful inspection of the cAFM measurement suggests that this shape change (from spot to ring) is actually due to SPM tip damage—if the tip edge erodes and the conductive channels in the film are small, then the conductive channel effectively probes the tip rather than vice versa.

We also examined the topography of cAFM measurements and found no topographic changes corresponding to the evolution of the conductive spots, as shown in Fig. 6. In our cAFM measurement, generally, we can see more conductive spots under higher V_{dc} (as shown in Fig. 4). Therefore, we speculate that these conductive spots are related to defects in the HZO film. We believe that there may exist an asperity in the film or underlying electrode that leads to local dielectric breakdown under the high applied fields and the formation of the conductive spots. Other possible features include grain boundaries, or locally high concentrations of oxygen vacancies.

This result differs from previous studies where the conductivity of HfO_2 based films was related to oxide diffusion, trap density, and dielectric thinning.[15,30–33] We suggest, however, that several different

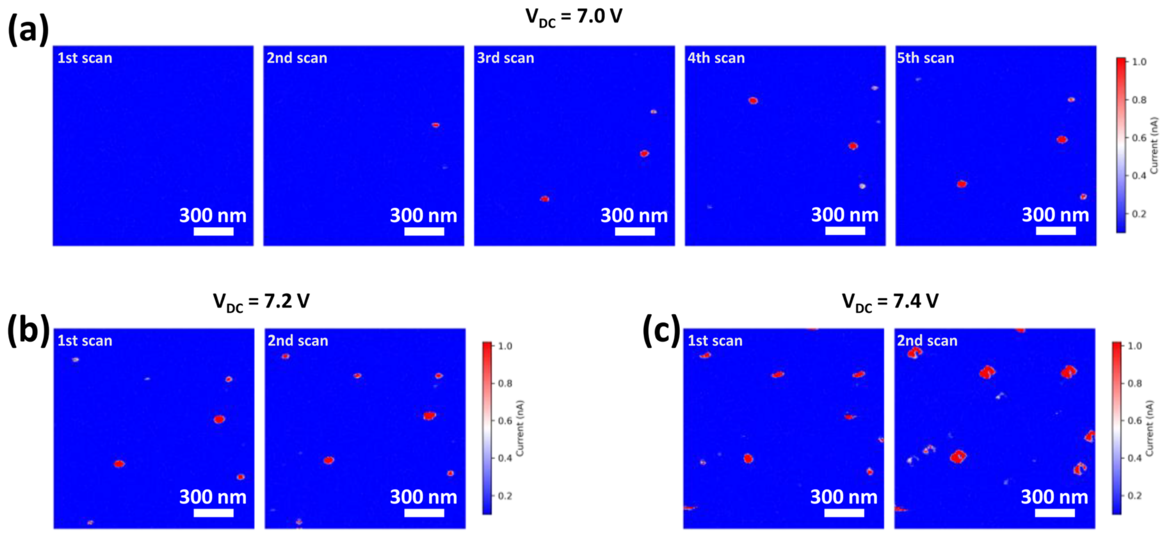

FIG. 4. The evolution of conductive spots as a function of applied DC voltage. (a) cAFM current images showing the evolution of conductive spots under continuous scan with a constant $V_{DC} = 7$ V. (b) The evolution of conductive spots under $V_{DC} = 7.2$ V. (c) The evolution of the conductive spots under $V_{DC} = 7.4$ V.

mechanisms lead to conductive spots formation and evolution (Fig. 3). The disappearance of conductive spots suggests that the material in the electric field changed during operation; it is unknown if these changes would impact a device in positive or negative ways, and it likely depends on the type of device of interest (e.g., resistive vs capacitive memory). Therefore, further study, e.g., investigating charge injection and retention,[34] is necessary to understand the mechanism of conductive spots in HZO films.

In summary, we developed a feature-exploration workflow for automated microscopy measurement. This workflow enables the exploration of specific features (e.g., conductive channel, defect, surface contamination, etc.) observable in microscopy images, based on a

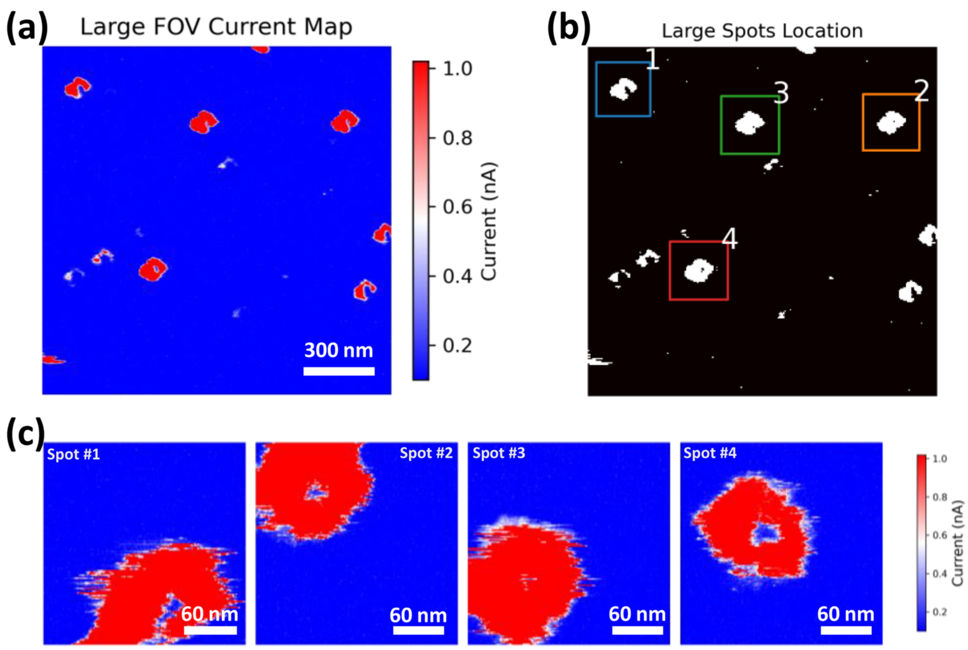

FIG. 5. FE-cAFM results for exploring the shape change of conductive spots. (a) A copy of the cAFM image shown in Fig. 4(c)-first scan, this image will be used as the large FoV image for the feature-exploration workflow. (b) Spot locations determined by the feature-exploration workflow. Here, we customize the workflow parameter (noise radius) to locate the relatively large spots. (c) Zoomed-in scan images showing the shapes of the conductive spots.

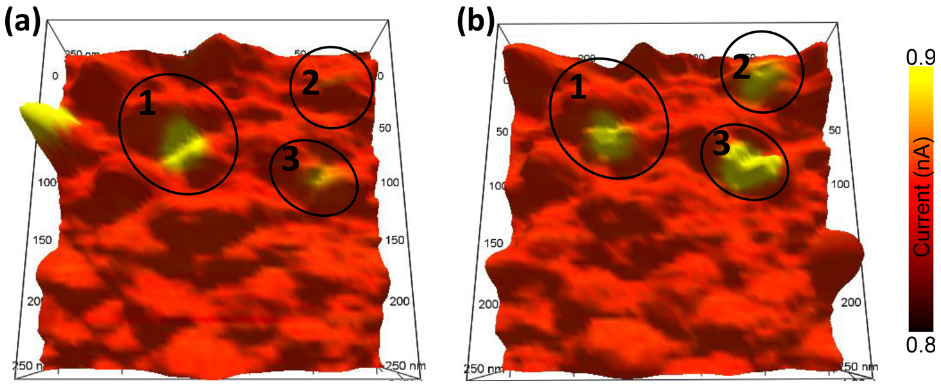

FIG. 6. Evolution of the conductive spots along with topography; the geography shows topography and the color shows current. (a) Original topography and current; (b) topography and current after continuous scans. (a) and (b) A distinct conductive spots change is shown, but there is no corresponding topographic difference. Note that there is an image drift during AFM measurement, so the correspondence between (a) and (b) is labeled.

large FoV microscopy image. Zoom-in measurements can be recorded in an automated manner. Integrating this feature-exploration workflow with conductive atomic force microscopy (FE-cAFM), we investigated the conductive spots in a HZO thin film. The FE-cAFM allowed us to explore the evolution of each conductive spots observed in a large FoV cAFM current image, revealing that the conductive spots appear, disappear, and/or reappear as a function of scan cycles and applied DC voltages. We discovered variable behaviors in the conductive spots, which may imply different formation mechanisms.

This feature-exploration workflow was of use anytime during microscopy measurement, except the very beginning of the measurement. It provided a useful alternative to human intervention in zoom-in measurements. This technology can be customized to focus on specific features with varying sizes. Nonetheless, the workflow can be further improved in the future, such as including functions to identify erroneous data, extending the workflow from imaging mode to spectroscopy mode. In addition, it can be implemented in SPM, electron microscopy, optical microscopy, and chemical imaging.

See the supplementary material for methods.

This work (material synthesis and automated experiment development) was primarily supported by the Center for 3D Ferroelectric Microelectronics (3DFeM), an Energy Frontier Research Center funded by the U.S. Department of Energy (DOE), Office of Science, Basic Energy Sciences under Award No. DE-SC0021118. The work (algorithm development and data analysis) was also supported by the Oak Ridge National Laboratory's Center for Nanophase Materials Sciences (CNMS), a U.S. Department of Energy, Office of Science User Facility. The authors acknowledge Stephen Jesse and Nina Balke for fruitful discussion. Note that this manuscript has been authored by UT-Battelle, LLC, under Contract No. DE-AC0500OR22725 with the U.S. Department of Energy. The United States Government retains and the publisher, by accepting the article for publication, acknowledges that the United States Government retains a non-exclusive, paid-up, irrevocable, world-wide license to publish or reproduce the published form of this manuscript, or allow others to do so, for the United States Government purposes. The Department of Energy will provide public access to these results of federally sponsored research in accordance with the DOE Public Access Plan (http://energy.gov/downloads/doe-public-access-plan).

AUTHOR DECLARATIONS

Conflict of Interest

The authors have no conflicts to disclose.

DATA AVAILABILITY

The data that support the findings of this study are available within the article and supplementary material.

REFERENCES

[1]L. W. Martin and A. M. Rappe, Nat. Rev. Mater. **2**(2), 16087 (2017).
[2]T. Mikolajick, S. Slesazeck, H. Mulaosmanovic, M. Park, S. Fichtner, P. Lomenzo, M. Hoffmann, and U. Schroeder, J. Appl. Phys. **129**(10), 100901 (2021).
[3]N. Setter, D. Damjanovic, L. Eng, G. Fox, S. Gevorgian, S. Hong, A. Kingon, H. Kohlstedt, N. Park, and G. Stephenson, J. Appl. Phys. **100**(5), 051606 (2006).
[4]J. F. Ihlefeld, D. T. Harris, R. Keech, J. L. Jones, J. P. Maria, and S. Trolier-McKinstry, J. Am. Ceram. Soc. **99**(8), 2537–2557 (2016).
[5]J. Choi, Y. Mao, and J. Chang, Mater. Sci. Eng.: R **72**(6), 97–136 (2011).
[6]T. Böscke, J. Müller, D. Bräuhaus, U. Schröder, and U. Böttger, paper presented at the 2011 International Electron Devices Meeting, 2011.
[7]T. Böscke, S. Teichert, D. Bräuhaus, J. Müller, U. Schröder, U. Böttger, and T. Mikolajick, Appl. Phys. Lett. **99**(11), 112904 (2011).
[8]D. Biswas, M. N. Singh, A. K. Sinha, S. Bhattacharyya, and S. Chakraborty, J. Vac. Sci. Technol. B **34**(2), 022201 (2016).
[9]Y. Cao, J. Shen, C. Randall, and L. Q. Chen, J. Am. Ceram. Soc. **97**(11), 3568–3575 (2014).
[10]W. Geng, X. Qiao, C. Zhao, D. Zheng, Y. Li, L. Zhang, K. Bi, Y. Yang, Y. Sun, and X. Chou, Ceram. Int. **47**, 24047 (2021).
[11]G. W. Pabst, L. W. Martin, Y.-H. Chu, and R. Ramesh, Appl. Phys. Lett. **90**(7), 072902 (2007).
[12]F. Hui and M. Lanza, Nat. Electron. **2**(6), 221–229 (2019).
[13]K. Kyuno, K. Kita, and A. Toriumi, Appl. Phys. Lett. **86**(6), 063510 (2005).
[14]V. Yanev, M. Rommel, M. Lemberger, S. Petersen, B. Amon, T. Erlbacher, A. J. Bauer, H. Ryssel, A. Paskaleva, and W. Weinreich, Appl. Phys. Lett. **92**(25), 252910 (2008).
[15]V. Iglesias, M. Porti, M. Nafría, X. Aymerich, P. Dudek, and G. Bersuker, J. Vac. Sci. Technol. B **29**(1), 01AB02 (2011).
[16]C. N. Lau, D. R. Stewart, R. S. Williams, and M. Bockrath, Nano Lett. **4**(4), 569–572 (2004).
[17]C. N. Lau, D. R. Stewart, M. Bockrath, and R. S. Williams, Appl. Phys. A **80**(6), 1373–1378 (2005).
[18]J. J. Yang, F. Miao, M. D. Pickett, D. A. Ohlberg, D. R. Stewart, C. N. Lau, and R. S. Williams, Nanotechnology **20**(21), 215201 (2009).
[19]K. Szot, W. Speier, G. Bihlmayer, and R. Waser, Nat. Mater. **5**(4), 312–320 (2006).
[20]O. S. Ovchinnikov, S. Jesse, and S. V. Kalinin, Nanotechnology **20**(25), 255701 (2009).

[21]K. P. Kelley, Y. Ren, A. N. Morozovska, E. A. Eliseev, Y. Ehara, H. Funakubo, T. Giamarchi, N. Balke, R. K. Vasudevan, and Y. Cao, ACS Nano **14**(8), 10569–10577 (2020).
[22]S. V. Kalinin, M. A. Ziatdinov, J. Hinkle, S. Jesse, A. Ghosh, K. P. Kelley, A. R. Lupini, B. G. Sumpter, and R. K. Vasudevan, arXiv:2103.12165 (2021).
[23]R. K. Vasudevan, K. P. Kelley, J. Hinkle, H. Funakubo, S. Jesse, S. V. Kalinin, and M. Ziatdinov, ACS Nano **15**(7), 11253–11262 (2021).
[24]Y. Liu, K. P. Kelley, R. K. Vasudevan, H. Funakubo, M. A. Ziatdinov, and S. V. Kalinin, arXiv:2108.06037 (2021).
[25]K. P. Kelley, Y. Ren, A. Dasgupta, P. Kavle, S. Jesse, R. K. Vasudevan, Y. Cao, L. W. Martin, and S. V. Kalinin, ACS Nano **15**(9), 15096–15103 (2021).
[26]K. P. Kelley, S. V. Kalinin, M. Ziatdinov, O. Paull, D. Sando, V. Nagarajan, R. K. Vasudevan, and S. Jesse, Appl. Phys. Lett. **119**(13), 132902 (2021).
[27]S. S. Fields, S. W. Smith, P. J. Ryan, S. T. Jaszewski, I. A. Brummel, A. Salanova, G. Esteves, S. L. Wolfley, M. D. Henry, and P. S. Davids, ACS Appl. Mater. Interfaces **12**(23), 26577–26585 (2020).
[28]S. S. Fields, D. H. Olson, S. T. Jaszewski, C. M. Fancher, S. W. Smith, D. A. Dickie, G. Esteves, M. D. Henry, P. S. Davids, and P. E. Hopkins, Appl. Phys. Lett. **118**(10), 102901 (2021).
[29]Y. Wu, Z. Fan, Y. Fang, and C. Liu, in IEEE/ASME Transactions on Mechatronics, 2021.
[30]S. Kumar, Z. Wang, X. Huang, N. Kumari, N. Davila, J. P. Strachan, D. Vine, A. D. Kilcoyne, Y. Nishi, and R. S. Williams, Appl. Phys. Lett. **110**(10), 103503 (2017).
[31]S. Kumar, Z. Wang, X. Huang, N. Kumari, N. Davila, J. P. Strachan, D. Vine, A. D. Kilcoyne, Y. Nishi, and R. S. Williams, ACS Nano **10**(12), 11205–11210 (2016).
[32]O. Pirrotta, L. Larcher, M. Lanza, A. Padovani, M. Porti, M. Nafría, and G. Bersuker, J. Appl. Phys. **114**(13), 134503 (2013).
[33]V. Iglesias, M. Porti, M. Nafría, X. Aymerich, P. Dudek, T. Schroeder, and G. Bersuker, Appl. Phys. Lett. **97**(26), 262906 (2010).
[34]R. Kumar, P. Gupta, and S. K. Sharma, Adv. Mater. Interfaces **8**(20), 2100529 (2021).